



High-frequency, year-round time series of the carbonate chemistry in a high-Arctic fjord (Svalbard)

Jean-Pierre Gattuso^{1, 2}, Samir Alliouane¹, and Philipp Fischer³

¹Sorbonne Université, CNRS, Laboratoire d’Océanographie de Villefranche, 181 chemin du Lazaret, F-06230 Villefranche-sur-mer, France

²Institute for Sustainable Development and International Relations, Sciences Po, 27 rue Saint Guillaume, F-75007 Paris, France

³Alfred-Wegener-Institut Helmholtz Centre for Polar and Marine Research, Kurpromenade 211, 27498 Helgoland, Germany

Correspondence: Jean-Pierre Gattuso (jean-pierre.gattuso@imev-mer.fr)

Abstract. The Arctic Ocean is subject to high rates of ocean warming and acidification, with critical implications for marine organisms as well as ecosystems and the services they provide. Carbonate system data in the Arctic realm are spotty in space and time and, until recently, there was no time-series station measuring the carbonate chemistry at high frequency in this region, particularly in coastal waters. We report here on the first high-frequency (1 h), multi-year (5 years) dataset of salinity, temperature, dissolved inorganic carbon, total alkalinity, CO₂ partial pressure (pCO₂) and pH at a coastal site (11 m) in a high-Arctic fjord (Kongsfjorden, Svalbard). We show that (1) the choice of formulations for calculating the dissociation constants of the carbonic acid remains unsettled for Arctic waters, (2) the water column is generally somewhat stratified despite the shallow depth, (3) the saturation state of calcium carbonate is subject to large seasonal changes but never reaches undersaturation (Ω_a ranges between 1.4 and 3.0) and (4) pCO₂ is lower than atmospheric CO₂ at all seasons, making this site a sink for atmospheric CO₂ (16.8 mol CO₂ m⁻² yr⁻¹).

1 Introduction

Despite their major importance, Arctic shelves are among the areas which are understood the least. The Arctic Ocean only covers 4.3% of the total ocean area but has a continental shelf considerably larger than other oceans (52.7% of its total area vs less than 18% globally; Jakobsson et al., 2004; Menard and Smith, 1966) and the total length of its coastline affected by the presence of permafrost represents around 34% of the world coastline (Lantuit et al., 2012). It contains less than 1% of ocean water but receives 11% of the global runoff (Shiklomanov, 1998) and is responsible for 7-10% of the global burial of organic carbon (Stein and Macdonald, 2004).

The Arctic region is one of the “reasons for concern” of the Intergovernmental Panel on Climate Change (IPCC; O’Neill et al., 2017). The Arctic Ocean exhibits the fastest and largest changes which already have impacts on the biota and biogeochemical cycles (Wassmann et al., 2010). The increase in sea surface temperature over the last two decades is similar to, or only slightly higher than, the global average (Fox-Kemper et al., 2021). However, the greatest future warming is in the Arctic



Ocean, where multi-model mean warming in 2080–2099 can exceed 2 to 5 °C relative to 1995–2014, depending on the CO₂ emissions scenario considered (Kwiatkowski et al., 2020).

25 The massive release of anthropogenic CO₂ also generates ocean acidification, a process that describes the increase in dissolved inorganic carbon and bicarbonate and the decline of pH and the saturation state of calcium carbonate minerals. The projected decrease in pH is projected to be larger in the surface Arctic Ocean than elsewhere, with model mean declines that can exceed 0.45 pH units in SSP5-8.5 (2080–2099 anomalies relative to 1995–2014)(Kwiatkowski et al., 2020).

30 Freshwater input via rivers and glacier melting have a profound impact on the seawater carbonate chemistry. It decreases total alkalinity, the seawater buffering capacity and the calcium carbonate saturation state (Fransson et al., 2015). Undersaturation of surface water with respect to aragonite-type CaCO₃ was first reported for 2008 in the Canada Basin, preceding other open ocean basins (Zhang et al., 2020). Much of Arctic shallow waters are undersaturated with respect to calcium carbonate, especially aragonite. This is due to the decrease of salinity resulting from increased river runoff and sea ice melt in the summer (Chierici and Fransson, 2009), and to the degradation of organic matter in runoff waters and shelf areas (e.g., Anderson et al., 2017). Aragonite undersaturation has consequences on aragonite-shelled organisms such as pteropods (e.g., Comeau et al., 2011).

35 The remoteness and harsh environmental conditions make it difficult to gather carbonate chemistry data in the Arctic, although some coastal sites are easily accessible year round. The goal of this paper is to provide the first high-frequency, multi-year dataset of salinity, temperature, dissolved inorganic carbon, total alkalinity, pCO₂ and pH.

2 Material and methods

40 Data were collected at the COSYNA/MOSES-AWIPEV underwater observatory operated since 2012 in Kongsfjorden, an Arctic fjord located on the west coast of Spitsbergen (Svalbard) at 78°55′50.37″ N and 11°55′12.10″ E (Fischer et al., 2017) (Fig. 1). The study site is coastal (11 m depth ± 0.7 m of tidal amplitude) and is relatively sheltered in the inner part of the Kongsfjorden, with average tidal currents of 0.1 m yr⁻¹. Kongsfjorden is a typical Arctic fjord with minimum winter water temperatures of -1.9 to 0.8 °C in February and March, and maximum average water temperatures of more than 6 °C in August (see Appendix A). Until 2006, the fjord was regularly covered by sea ice in winter (Gerland and Renner, 2007). Before 2006, 45 the sea ice typically extended into the central part of the fjord, but during the last decade the sea-ice extent has often been reduced to the northern part of the inner bay (Pavlova et al., 2019).

2.1 The COSYNA/MOSES-AWIPEV observatory

The COSYNA/MOSES-AWIPEV underwater observatory comprises a land-based FerryBox system (Fig. 1a) equipped with a set of sensors (Table 1). The FerryBox receives water from 11 m depth from an underwater pump (Fig. 1b and c). To prevent for 50 biofouling of the sensors, every night at 00:10, a sulfuric acid (4% for 10 min) flush of the entire sensor system was followed by a rinse with freshwater (30 min) prior to switching again to measuring mode. The observatory also comprises a profiling sensor carrier fitted with another set of sensors that can be remotely-controlled (Fig. 1d and Table 1). The profiling unit is positioned in one of the following distances from the sea bottom 1, 3, 5, 7 or 9 m. The effective water depth of the system changed with

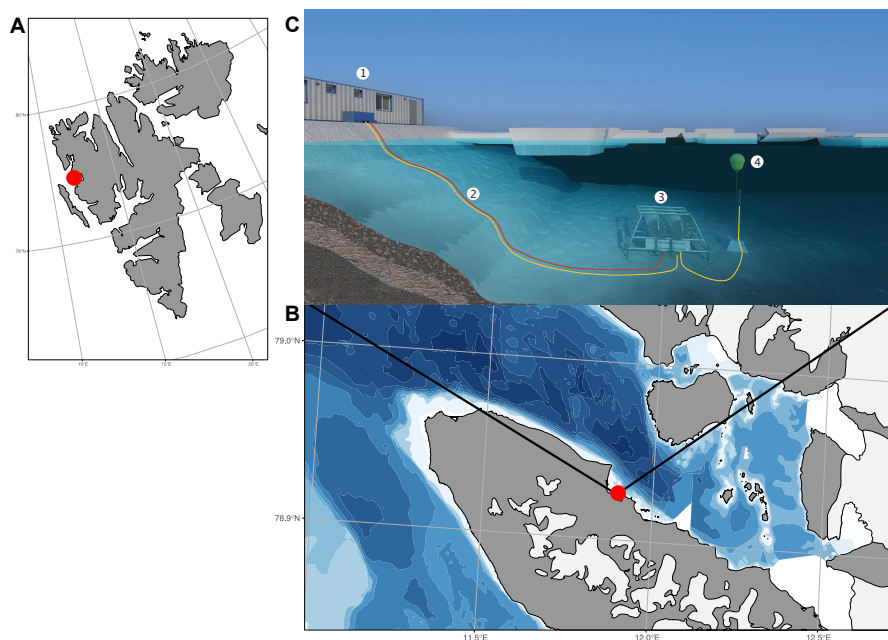


Figure 1. Svalbard (A), Kongsfjorden and Ny-Ålesund (B), and observational set-up. a: FerryBox system, b: underwater cable and underwater tubes for water supply for FerryBox system, c: underwater node with water pumps and d: underwater sensor systems with profiling unit. The maps were produced by the R package ggOceanMaps (Vihtakari, 2022).

the tide cycle for at most 1.5 m, but the system itself had a fixed position above ground. For a more detailed description of the
55 Svalbard underwater observatory see Fischer et al. (2017) and Fischer et al. (2020).

2.2 Discrete sampling and measurements

Seawater was sampled in the FerryBox, at about weekly frequency. It was collected into duplicate 500 ml borosilicate glass
bottles after a careful rinse. Samples were immediately poisoned with mercuric chloride as described by Dickson et al. (2007).
Dissolved inorganic carbon (C_T) and total alkalinity (A_T) were analysed within 6 months via potentiometric titration following
60 methods described by Edmond (1970) and DOE (1994), by Service National d'Analyse des Paramètres Océaniques du CO_2 at
Sorbonne University, France. Unless flagged as of poor quality, C_T and A_T of replicate bottle samples were averaged. When
the difference between duplicates was larger than $10 \mu\text{mol kg}^{-1}$, the replicate closer to the general trend was kept and the other
discarded. The number of outliers discarded was 38 and 41, respectively for C_T and A_T .

Starting in November 2018, seawater was sampled at approximately monthly interval for pH measurements both in the
65 FerryBox and in the field, below 8 m with a Niskin bottle, to calibrate the pH sensors. Samples were preserved as described
by Dickson et al. (2007). pH was measured spectrophotometrically within 6 months of sampling as described in Dickson et al.
(2007) using purified m-cresol purple (purchased from Robert H. Byrne's laboratory, University of South Florida). Three to
four replicate measurements were performed for each sample on a Cary 60 UV-Vis spectrophotometer (Agilent Technologies).



Table 1. Sensors deployed in the FerryBox and profiling system. All sensors in the FerryBox system are maintained once a year and all sensors of the profiling system are changed once a year and sent to the manufacturer for maintenance and calibration. The salinity sensors were calibrated according to the standard Unesco procedure (IOC et al., 2010).

Location	Parameters and sensors	Year of installation
FerryBox	Water temperature ($^{\circ}\text{C}$), SeaBird SBE45	2012
	Conductivity (ms m^{-1}) / Salinity, SeaBird, SBE45	2012
	Oxygen (%), Aanderaa 4175C	2012
	Chl-a (mg m^{-3}), Seapoint Chlorophyll Fluorometer	2012
	Turbidity (FTU), SeaPoint turbidity meter	2012
	Partial pressure of CO_2 (μatm), Kongsberg Maritime, HydroC CO2 FT	2015
Profiling system	Pressure (dbar), Sea&Sun CTD90	2012
	Water temperature ($^{\circ}\text{C}$), SBE 38 Digital Oceanographic Thermometer	2015
	Conductivity (ms m^{-1}) / Salinity, Sea&Sun CTD90 - ADM 7 pole electrode cell	2012
	Oxygen (%), Sea&Sun CTD90 - Aanderaa 4175C	2012
	Chl-a (mg m^{-3}), Sea&Sun CTD90 - Cyclops7 Fluorometer	2012
	Turbidity (FTU), Sea&Sun CTD90 - Seapoint turbidity meter	2012
	Photosynthetically available radiation (SeaBird), ECO-PAR	2015
	pH (total scale), SeaBird SeaFET	2017

Repeatability was very good: the standard deviation of the replicates ranged from 0.00033 to 0.0091 pH units and the average of 44 mean standard deviations was 0.002 pH units.

2.3 Partial pressure of CO_2

The measuring range of the HydroC CO_2 FT sensor (Contros Kongsberg Maritime) is 200-1000 μatm , resolution is $< 1 \mu\text{atm}$ and accuracy is $\pm 1\%$ reading. The sensor was positioned first in the loop of sensors of the FerryBox in order to avoid alteration of pCO_2 through exposure to air. Two sensors were swapped every year and while one was monitoring pCO_2 , the other one was factory-calibrated. pCO_2 was measured continuously and data logged every minute. Calibration of the unit was performed by the supplier. It comprised a post-deployment calibration (to assess the drift), a general maintenance, including a change of membrane, and a pre-deployment calibration. This two-step calibration was used to correct the pCO_2 data as described by the supplier. Data collected after 2020-03-01 were not used because the Covid-19 pandemic prevented maintenance and the setup of a freshly calibrated sensor. As a result, algae became increasingly abundant, pulling pCO_2 down and further away from values calculated from C_T and A_T . pCO_2 was expressed at *in situ* temperature using the pCO_2insi function of the R package seacarb (Gattuso et al., 2021).



Table 2. Data quality flags.

Flag	Description	Example
1	Good data	Data not matching any of the other flags
3	Failing the date and time test	Data with impossible date (date outside of the project period)
4	Data not usable according to manufacturer	Data recorded during instrument flush or zeroing period
7	Failing the regional range test	Data out of range (e.g. salinity > 37)
12	Failing the spike test using the despiking function of the R package oce Kelley and Richards (2021) with n=2 and k=5761	Data assigned with NA as a result of the spike test
15	Instrument not deployed or operated	Data assigned with NA when the instrument is in maintenance
16	Data impacted by acid flush	Data still stabilizing after an acid flush (each day between 24:00 01:00)
99	Failing the final visual inspection	Data considered as outlier by visual inspection

2.4 pH

Two SeaFET Ocean pH sensors (Sea-Bird Scientific) were swapped on 2018-04-17, and 2019-09-02. While one was monitoring pH and temperature on the profiler, the other one was factory-calibrated. pH (volts) was measured continuously and data logged every minute. Volts values measured below 8 m in each of the three deployment periods were converted to pH on the total scale (pHT). Field calibration samples for pH were collected using a Niskin bottle close to SeaFET within 15 min of measurement. pH was measured spectrophotometrically (Dickson et al., 2007) with purified m-cresol purple (purchased from Robert H. Byrne's laboratory, University of South Florida). Calibration was performed as described by Bresnahan et al. (2014) using the functions sf_calib and sf_calc of the R package seacarb (Gattuso et al., 2021). The pHinsi function of the R package seacarb v3.3.0 (Gattuso et al., 2021) was used to express pH at temperatures other than the measurement temperature from pH, salinity, and total alkalinity. The dissociation constants used are discussed below.

2.5 Data flow and quality insurance

Data collected at one minute frequency were assigned with quality flags following a series of quality tests (Table 2). Data with flags other than 1 (good data) were eliminated and outliers removed using despiking function of the R package oce (Kelley and Richards, 2021) prior to calculating hourly averages.



2.6 Calculation of derived parameters of the carbonate system

The carb function of the R package seacarb v3.3.0 (Gattuso et al., 2021) was used to calculate all parameters of the carbonate system from pairs of measured variables (e.g., C_T and A_T , pCO_2 and A_T , pH and C_T ...), salinity, temperature and hydrostatic pressure. Total boron concentration was calculated from salinity (Lee et al., 2010). The following constants were used: K_f from Perez and Fraga (1987) and K_s from Dickson (1990). The choice of the stoichiometric dissociation constants K_1^* and K_2^* is not obvious in polar oceans (Sulpis et al., 2020). Several sets of formulations were tested: Lueker et al. (2000), Millero et al. (2002), Papadimitriou et al. (2018) and Sulpis et al. (2020). Nutrient data (phosphate and silicate) were taken into consideration whenever available (van de Poll, unpublished data).

All parameters are reported at *in situ* temperature unless indicated otherwise. The average uncertainties of the derived carbonate parameters were calculated according to the Gaussian method (Dickson and Riley, 1978) implemented in the “errors” function of the R package seacarb (Orr et al., 2018; Gattuso et al., 2021). The uncertainties when using the A_T - C_T pair are $\pm 2.7 \times 10^{-10}$ mol H^+ (about 0.015 units pH_T), ± 15 μatm pCO_2 , and ± 0.1 unit for the aragonite and calcite saturation states. The maximum additional uncertainty associated with the unavailability of nutrient concentrations (P and Si) as input parameters is comparatively negligible (up to 0.0019 pH units, 1.5 μatm pCO_2 and 0.008 Ω_a units).

2.7 Air-sea CO_2 fluxes

The instantaneous air-sea CO_2 fluxes were calculated as described by De Carlo et al. (2013) from measured pCO_2 , atmospheric CO_2 measured at the Zeppelin station, also located at Ny-Ålesund (data downloaded on 2020-08-19 from <https://gaw.kishou.go.jp/search/file/0054-6001-1001-01-01-9999>, and the wind speed measured by the AWI at a height of 10 m (Maturilli, 2020). The gas exchange parameterization as a function of wind speed of Ho et al. (2006) was used.

3 Dataset and discussion

3.1 Data availability

It is often mentioned that there are fewer observations in the Arctic Ocean than elsewhere but it is not the case for carbonate variables. We looked at pCO_2 records in the v2022 version of the SOCAT database (Bakker et al., 2016) and the dissolved inorganic carbon (C_T) records of the GLODAP v2.2022 database (Lauvset et al., 2022). About 12.4% of the SOCAT pCO_2 records and 11.1% of the GLODAP C_T records are from the Arctic ocean as defined by the Organization (1953) which is only about 4.3% of the global ocean surface area. Coastal (bottom depth < 200 m) data are relatively well represented in both products (24.3% and 11.1% of the SOCAT and GLODAP total Arctic data, respectively). The monthly distribution is however very uneven with 71.2% of the SOCAT pCO_2 data and 71% of the GLODAP C_T data collected in four months of the year (June to September). Furthermore, few to very few data are available for December to March, including in coastal regions. To our knowledge, there is until today no high-frequency, multi-year time-series data.

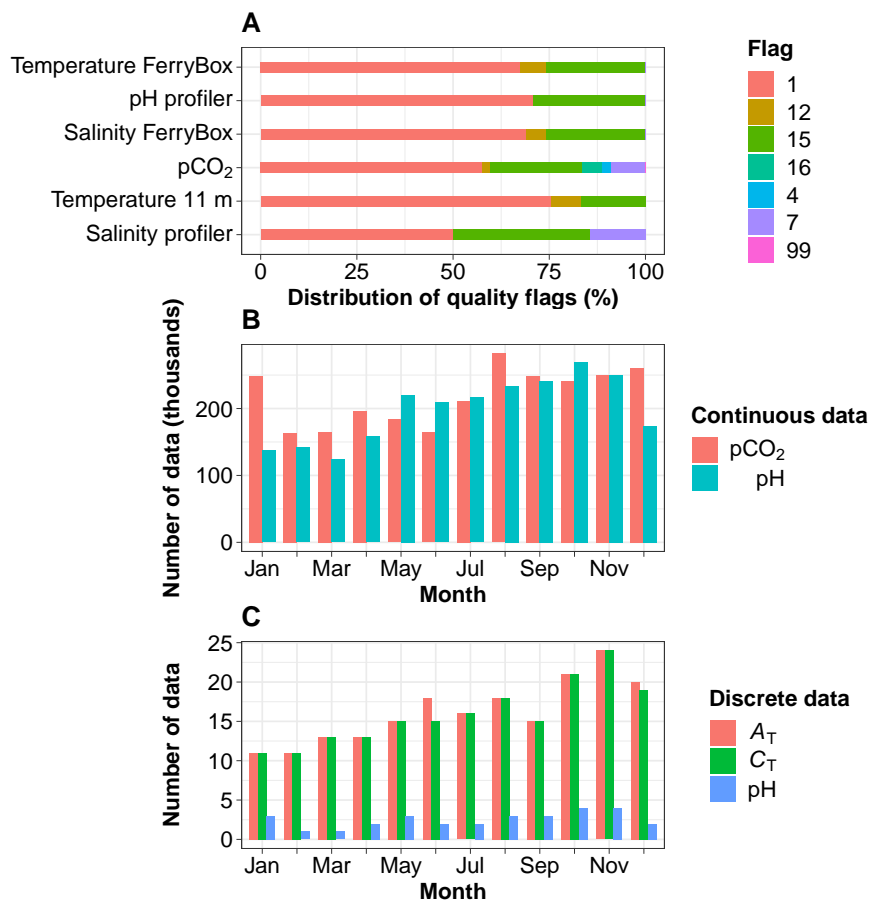


Figure 2. A: Distribution of the quality flags assigned to data collected every minute over the period July 2015 to December 2020, except for pH profiler sensor (SeaFET) which was set-up in August 2017. B: monthly distribution of pCO₂ and pH data. C: monthly distribution of discrete measurements of A_T, C_T and spectrophotometric pH. Flags are defined in Table 2.

The extreme environmental conditions prevailing at the study site incurred incidents such as interrupted supply of seawater in the FerryBox due to frozen pipes or damages resulting from icebergs pounding on the field instruments. Resolutions of these incidents sometimes took weeks to months due to waiting for warmer temperatures to make deicing possible or to delays bringing technical staff, including divers, to repair damages. The study site was not accessible for extended periods of time during the Covid-19 pandemic, preventing discrete sampling resulting in data gaps. The lack of sensor maintenance sometimes generated data of poor quality which were eliminated, also generating gaps. Nevertheless, data were usable 50 to 76% of the time during the period of measurement (Fig. 2A). Continuous pCO₂ and pH data are available throughout a composite year and well distributed across months, including in winter months (Fig. 2B). The total number discrete data available for A_T, C_T and spectrophotometric pH is 195, 191 and 30. They are also well distributed across months (Fig. 2C).



135 3.2 Impact of the formulations of K_1^* and K_2^*

Chen et al. (2015) found that the constants of Mehrbach et al. (1973) and Lueker et al. (2000) yield the best internal consistency in Arctic waters over the temperature range of $-1.5 \leq T \leq 10.5$ °C and salinity range of $25.8 \leq S \leq 33.1$. They recommended the use of these constants. Sulpis et al. (2020) have shown that current estimates of K_1^* and K_2^* are inconsistent with measured CO₂ system parameters in cold oceanic region. The formulations of Lueker et al. (2000, L00), which are recommended by the community (Jiang et al., 2022), were derived in laboratory conditions with no temperature value below 2 °C. These formulations overestimates the stoichiometric dissociation constants at temperatures below about 8 °C (Sulpis et al., 2020). There are several alternative formulations. Those of Millero et al. (2002, M02) and (Sulpis et al., 2020, S20) are based on large (> 900) field data that include cold temperature values. The formulations of Papadimitriou et al. (2018, P18), obtained in the laboratory, also cover cold temperatures.

145 3.2.1 Using the pair $p\text{CO}_2$ - A_T

For the pair $p\text{CO}_2$ - A_T (115 data pairs), it is the formulation of P18 which provides estimates of pH and C_T closest to those obtained with L00 (Fig. 3). The absolute median difference between L00 and P18 are significantly smaller than the uncertainty estimated by error propagation for pH (0.001 vs 0.004 units) and C_T (1.7 vs 3.6 $\mu\text{mol kg}^{-1}$). The formulation of M02 performs well for C_T (1.5 vs 3.6 $\mu\text{mol kg}^{-1}$) but less well for pH (0.019 vs 0.004 units). The absolute median difference between L00 and S20 is similar to the uncertainty estimated by error propagation for C_T (3.7 vs 3.6 $\mu\text{mol kg}^{-1}$) but is more than six times larger for pH (0.026 vs 0.004 units). For all formulations, the uncertainty for the saturation state for aragonite is negligible and smaller than that estimated with the propagation of errors.

3.2.2 Using the pair A_T - C_T

The discrete values of A_T , C_T , salinity and temperature in the FerryBox were used to calculate pH using the same formulations for K_1^* and K_2^* as above (Fig. 3). Overall, the absolute median difference between the formulation of L00, on one hand, and S20, P18 and M02, on the other hand, is lowest with P18. The absolute median difference L00-P18 is small compared to the overall uncertainty estimated by error propagation: 0.004 vs 0.013 pH units and 3.1 vs 10.9 $\mu\text{atm pCO}_2$.

3.2.3 Measured pH vs pH calculated from $p\text{CO}_2$ and A_T

Here we compare pH measured spectrophotometrically with pH calculated from $p\text{CO}_2$ and A_T using various formulations of K_1^* and K_2^* (Table 3). All pH values were normalized to a temperature of 4 °C. The absolute differences are up to 0.11 pH units. In general, all formulations overestimate spectrophotometric pH. pH calculated using the formulation of Lueker et al. (2000) is closer to measured pH, with a mean difference of -0.029 pH units. This difference is almost 9 times larger than the uncertainty for pH calculated from $p\text{CO}_2$ and A_T estimated by error propagation (0.004 units). The next closer formulation is Papadimitriou et al.'s.

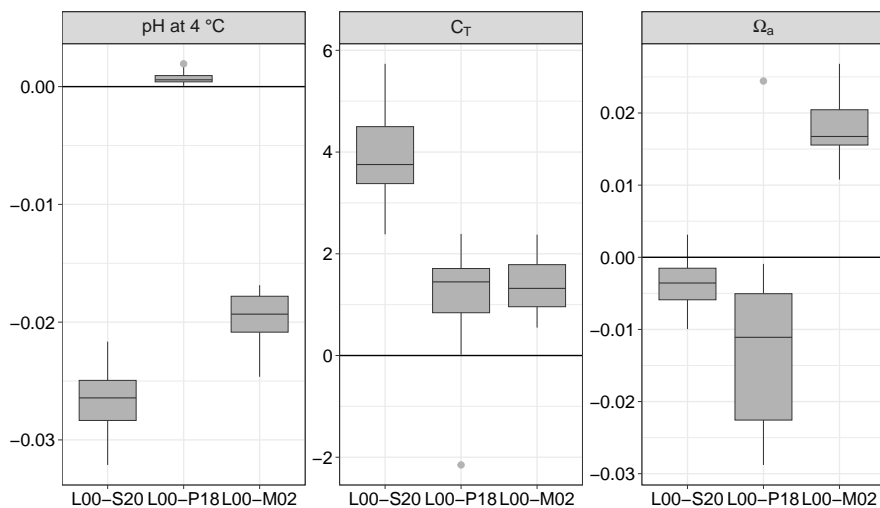


Figure 3. pH normalised at 4 °C, dissolved inorganic carbon (C_T) and saturation state of aragonite Ω_a calculated from pCO_2 and A_T (115 data pairs): differences between the formulations for K_1 and K_2 of Lueker et al. (2000, L00) and those of Sulpis et al. (2020, S20), Papadimitriou et al. (2018, P18) and Millero et al. (2002, M02). Unit for C_T is $\mu\text{mol kg}^{-1}$.

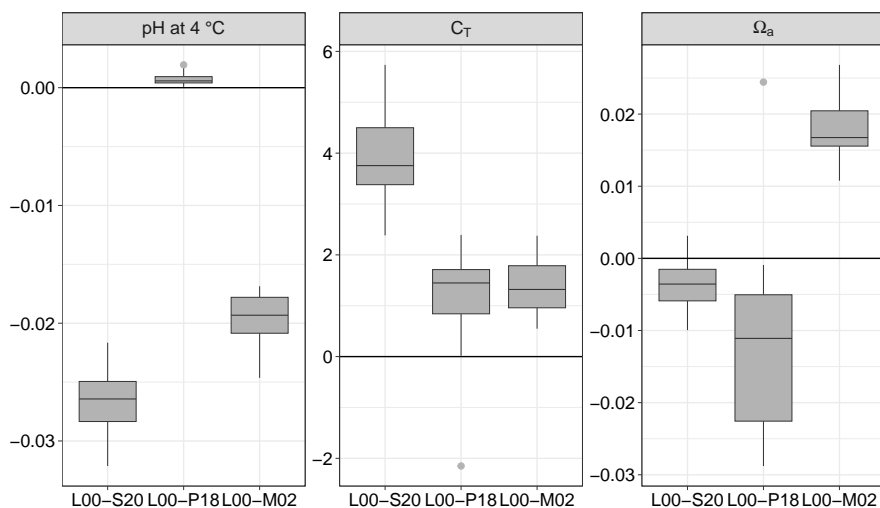


Figure 4. pH normalised at 4 °C, partial pressure of CO_2 and saturation state of aragonite Ω_a calculated from A_T and A_T (115 data pairs): differences between the formulations for K_1 and K_2 of Lueker et al. (2000, L00) and those of Sulpis et al. (2020, S20), Papadimitriou et al. (2018, P18) and Millero et al. (2002, M02). Units for pCO_2 is μatm .



Table 3. Difference between spectrophotometric pH and pH calculated with $p\text{CO}_2$ and A_T using different formulations for K_1^* and K_2^* .

	Lueker et al. (2000)	Sulpis et al. (2020)	Papadimitriou et al. (2018)	Millero et al. (2002)
Minimum	-0.086	-0.108	-0.083	-0.110
Q1	-0.036	-0.069	-0.042	-0.056
Median	-0.026	-0.060	-0.033	-0.046
Mean	-0.029	-0.059	-0.032	-0.049
Q3	-0.020	-0.045	-0.019	-0.041
Maximum	0.012	-0.029	0.000	-0.007

165 3.2.4 Measured pH vs pH calculated from A_T and C_T

Here we compare pH measured spectrophotometrically with pH calculated from discrete measurements of C_T and A_T using various formulations of K_1^* and K_2^* (Table 4). All pH values were normalized to a temperature of 4 °C. The absolute differences can be as high as 0.133 pH units. In general, all formulations overestimate spectrophotometric pH. pH calculated using the formulations of Lueker et al. (2000) and Papadimitriou et al. (2018) are closer to measured pH, with absolute median differences of -0.007 pH units. This difference is much smaller than the uncertainty for pH calculated from A_T and C_T according to seacarb (0.013). The mean differences found with the other formulations are slightly lower than the uncertainty for pH calculated from A_T and C_T according to seacarb.

Table 4. Difference between spectrophotometric pH and pH calculated with A_T and C_T using different formulations for K_1^* and K_2^* .

	Lueker et al. (2000)	Sulpis et al. (2020)	Papadimitriou et al. (2018)	Millero et al. (2002)
Minimum	-0.112	-0.133	-0.113	-0.129
Q1	-0.032	-0.048	-0.030	-0.049
Median	-0.007	-0.027	-0.007	-0.024
Mean	-0.015	-0.034	-0.014	-0.031
Q3	0.007	-0.015	0.007	-0.010
Max	0.081	0.064	0.087	0.065

In conclusion, with the exception of pH estimated with the $p\text{CO}_2$ - A_T pair, the formulations of Papadimitriou et al. (2018) performs better on our data set. It is, however, seldom used and the *de facto* standard has become the formulations of Lueker et al. (2000), which we have used in the present study. This issue needs to be revisited.



3.3 Impact of nutrient concentrations

Phosphate (PO_4) and silicate (Si) contribute to total alkalinity. Changes in their concentration can significantly affect calculations of the carbonate chemistry. The impact on our calculations was checked with a time series of nutrients comprising 90 phosphate and 133 silicate data kindly provided by van de Poll (unpubl. data). At the study site, the concentrations of PO_4 and Si vary by a factor 10 along a composite year. They range between 0.07 and 0.69 $\mu\text{mol kg}^{-1}$ for PO_4 and between 0.42 and 4.7 $\mu\text{mol kg}^{-1}$ for Si. In our dataset, disregarding the nutrient concentrations does not generate large differences in the derived parameters. Using the pCO_2 - A_T pair of variables, the absolute differences in pH, C_T and Ω_a are respectively 0.0001 unit, 0.7 $\mu\text{mol kg}^{-1}$ and 0.001. With the C_T - A_T pair, the absolute differences in pH, pCO_2 and Ω_a are 0.002 units, $< 1.5 \mu\text{atm}$ and < 0.01 .

185 3.4 Relationship between total alkalinity and salinity

The relationship between the total alkalinity (A_T) and salinity (S) is good (Fig. 5A). The equation of the ordinary least square linear regression is $A_T = 47.6 + 643 \times S$ ($r^2 = 0.81, N = 181$). The root mean square error (rmse) is 16.8 $\mu\text{mol kg}^{-1}$. Hunt et al. (2021) reported significant seasonal shifts in linear A_T vs S relationships on the East coast of the USA, demonstrating potential problems with any single linear model for the retrieval of A_T from salinity. There is no obvious seasonal shift in our data set. Splitting the data and regressing separately with salinity values below and above 34.5, as done by Nondal et al. (2009) for Nordic open ocean waters, does not prove useful (data not shown). It degrades r^2 (0.74 and 0.3 vs 0.81), and degrades or marginally improves the rmse (19 and 13.6 vs 16.8 $\mu\text{mol kg}^{-1}$). The relationship above was therefore used to estimate A_T from salinity.

3.5 Consistency of measured vs calculated pCO_2

195 The relationship between the measured and calculated pCO_2 (blue line) is relatively poor (Fig. 5B). The slope is 1.12 and its 95% confidence interval includes 1. The equation of the major axis regression is: Calculated pCO_2 (μatm) = $-23.5 + 1.14 \times$ Measured pCO_2 ($r^2 = 0.66, N = 95$)

3.6 Calibration of SeaFET pH sensors and consistency of measured vs calculated pH

200 The offset between the spectrophotometric reference samples and the calibrated SeaFET pH time series must be between -0.2 and 0.2 pH units (McLaughlin et al., 2017). The mean offset was ± 0.0026 units, with only one data point outside the recommended range, indicating a high-quality pH dataset (Fig. 5).

The relationship between spectrophotometric pH and SeaFET pH (blue line) is relatively good (Fig. ??D). The slope is 0.869 and its 95% confidence interval includes 1. The equation of the major axis regression is: SeaFET pH = $1.06 + 0.869 \times$ spectrophotometric pH ($r^2 = 0.89, N = 16$).

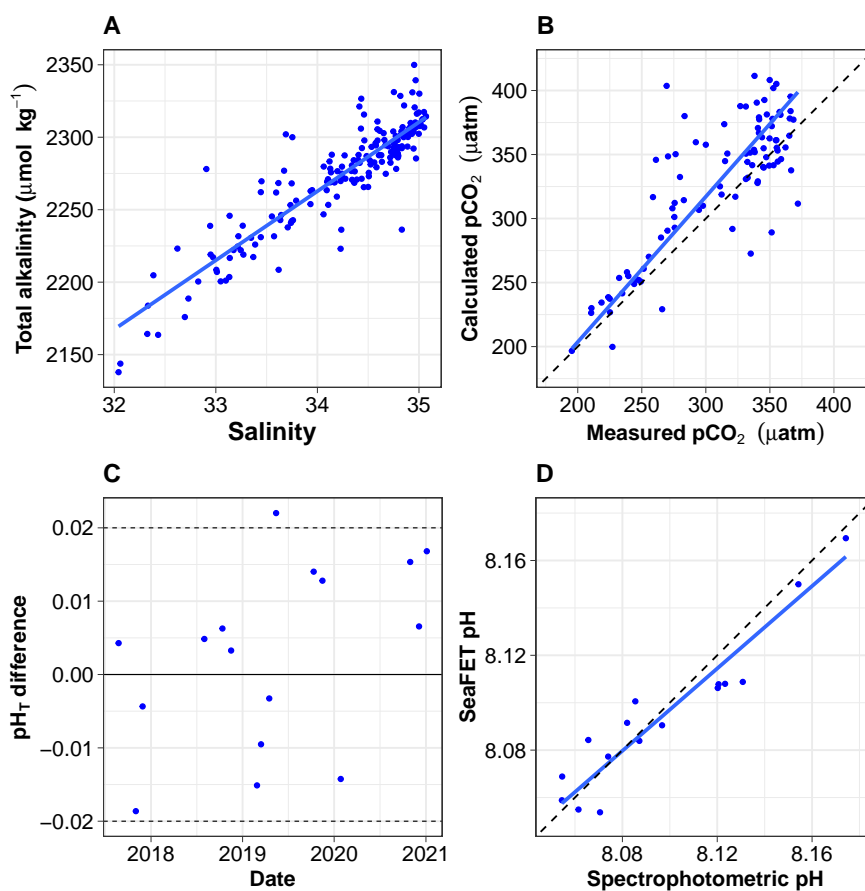


Figure 5. Relationship between discrete total alkalinity and salinity; the regression line is estimated using ordinary least square regression. B: pCO_2 calculated from A_T and C_T vs pCO_2 measured using the Contros sensor. All data are normalized at *in situ* temperature. The black dotted line is the 1:1 line while the blue solid line is calculated using a major axis regression. C: Offset (total scale) between spectrophotometric measurements of pH and the calibrated SeaFET pH time series. D: SeaFET pH vs spectrophotometric pH. All data on the total scale and normalized at *in situ* temperature. The black dotted line is the 1:1 line while the blue solid line is calculated using a major axis regression.

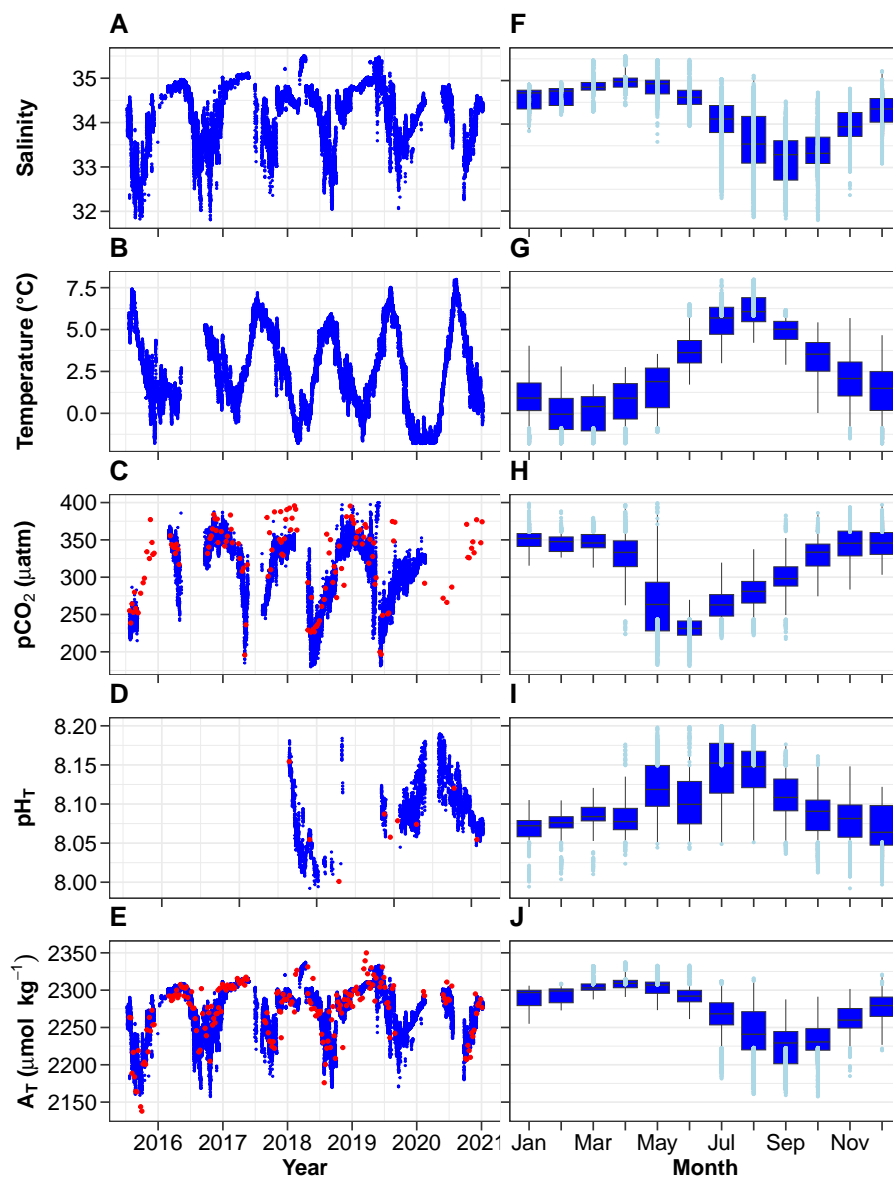


Figure 6. A-E: Time-series (A-E) and monthly distribution (F-J) of key environmental parameters (hourly means). In panels F-J, the orange lines [to add] indicate the medians, boxes show the first and third quartiles and the interquartile range; whiskers extend to the 5–95th percentiles. The light blue circles highlight values above the 90th percentile and below the 10th percentile.



205 3.7 Time series and monthly distribution of key parameters

The changes in salinity, temperature, partial pressure of CO₂, pH and total alkalinity are shown in Fig. 6A-E and monthly box plots in Fig. 6F-J. Salinity below 8 m is highest in the spring and lowest in the fall with monthly median values of 35 and 33.3, respectively. Positive salinity extremes (values > 90th percentile) mostly occur in March-June, presumably due to intrusion of seawater from the open sea. Negative salinity extremes (values < 10th percentile) are mostly observed in the summer (defined here as 3 months from June to August) and early fall, periods during which numerous streams release freshwater in the coastal zone. Temperature at 11 m is lowest in February and highest in August with monthly median values of -0.1 and 6.1 °C.

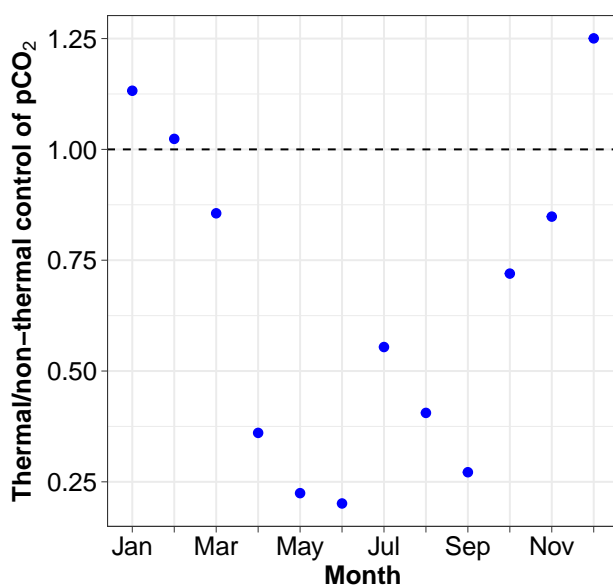


Figure 7. Ratio of the thermal vs non-thermal control of pCO₂.

pCO₂ at 11 m is almost always lower than 400 μatm with low values during and following the spring phytoplankton bloom and high values in winter. The relative importance of thermal and non-thermal (physical and biological) processes in controlling pCO₂ was investigated as described by Takahashi et al. (2002). The thermal/non-thermal ratio is lower than 1 for 9 months of a composite year, indicating that non-thermal drivers exert a greater control than temperature (Fig. 7). The ratio is above 1, hence thermal control is predominant, only in the three winter months of December, January and February.

3.8 Depth distribution

There is no depth profile of the variables in the usual sense as the REMOS profiler made stops for 24 h at specific depths to assess the biota in the water column (Fischer et al., 2017). However, the depth distribution of the median monthly salinity, temperature, density and pH provide useful information (Fig. 8). Salinity in the bottom layer (8 to 12 m) is up to 0.9 units



225 higher than in the surface layer (0 to 4 m) in summer, 0.6 units lower in December and relatively similar in both layers at other times. Temperature is lower by up to 2 °C in the deep layer from January to October and higher by up to 0.3 °C in November and December. Seawater density is always higher in the bottom than in the surface layer (up to 1.2 kg m⁻³ in July). The 12 m high water column is therefore generally stratified. This is a well-known feature, particularly in the Arctic due to low-salinity surface waters (Dong et al., 2021; Miller et al., 2019).

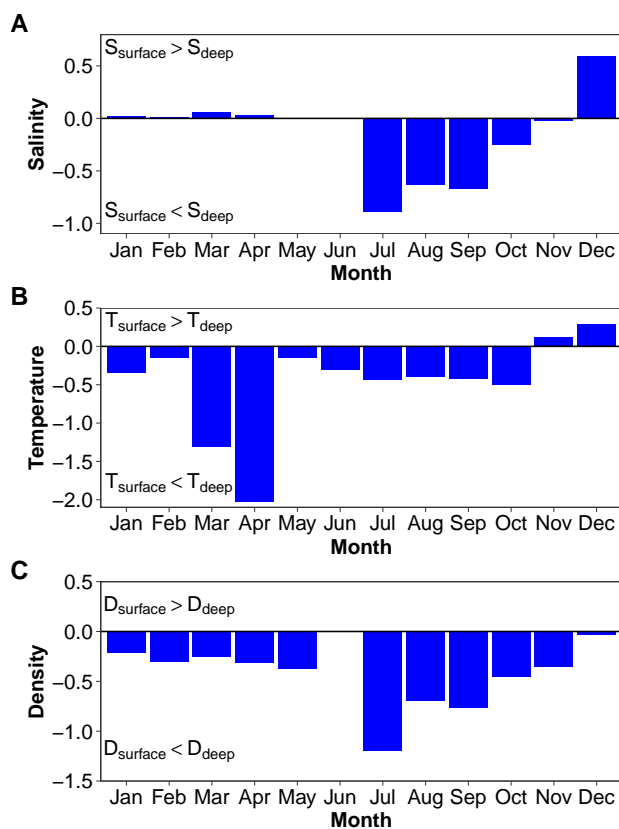


Figure 8. Vertical gradients calculated using the median monthly values of salinity (a), temperature (b) and density (c). "Surface" is 0 to 4 m and "deep" is 8 to 12 m.

3.9 Air-sea CO₂ fluxes

pCO₂ of seawater pumped at 11 m depth was measured in the FerryBox. This is not the best arrangement to estimate air-sea CO₂ fluxes considering the fact that the water column was sometimes stratified as shown by vertical gradient of salinity, temperature and density (Fig. 8). This is known to have consequences on the air-sea CO₂ flux. pCO₂ is generally higher in the bottom layer than in the surface layer (note that no data is available in May, June and July). To estimate air-sea CO₂ fluxes, pCO₂ can also be calculated using water-column variables measured or estimated from sensors attached to the REMOS



device: SeaFET pH, temperature, salinity and salinity-derived total alkalinity. At *in situ* temperature, the vertical gradient is within $\pm 4 \mu\text{atm}$, except in April where it is more than $40 \mu\text{atm}$ (Fig. 9A). Normalising pCO₂ at 4 °C (Fig. 9B) reduces the April difference from -45 to -22.6 μatm , indicating that the vertical gradient is partly driven by temperature.

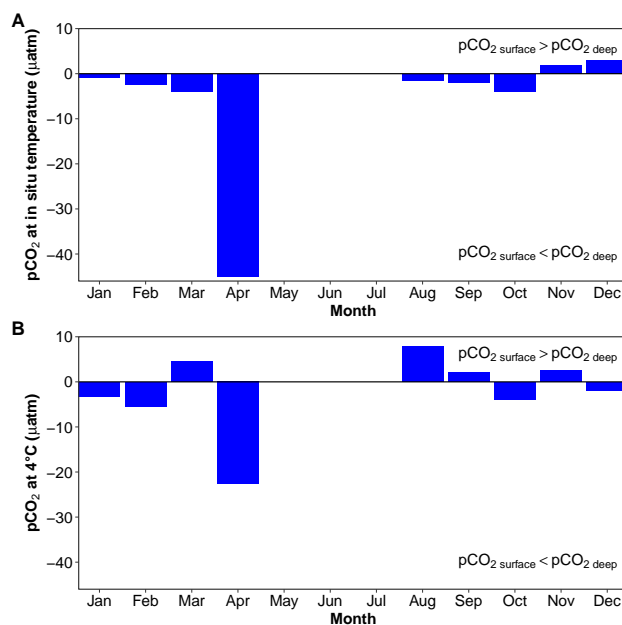


Figure 9. Vertical gradients estimated using the median monthly values of pCO₂ at *in situ* hydrostatic pressure, calculated from A_T (using the A_T vs S relationship) and SeaFET pH_T using the R package seacarb (Gattuso et al., 2021). A: CO₂ at *in situ* temperature; B: pCO₂ normalised at 4 °C. “Surface” is 0 to 4 m while “deep” is 8 to 12 m.

235 For the 9 months when data are available, monthly median pCO₂ at 11 m normalized at *in situ* temperature is well correlated with pCO₂ at 0 to 4 m ($r^2 = 0.81$) but it overestimates surface pCO₂ by a median value of 17 μatm (Fig. 10). Dong et al. (2021) have reported an even larger near-surface stratification of pCO₂ in sea-ice melt regions of the open Arctic Ocean. Surface values are consistently lower than bulk (~6 m) values by an average of 39 μatm , mostly due to fresher and colder melt waters, biasing near-surface stratification estimates of air-sea CO₂ flux.

240 The air-sea CO₂ flux is negative, indicating a CO₂ influx from the atmosphere, every month of a composite year (Fig. 11). The annual air-sea flux is 20 mol m⁻² yr⁻¹. Correcting for the underestimation of 17 μatm discussed above leads to a flux of -17 mol m⁻² yr⁻¹. The Arctic Ocean stands out as the region with the strongest CO₂ uptake per unit area during the period 1985–2019, with $-2.336 \pm 0.104 \text{ mol C m}^{-2} \text{ yr}^{-1}$ for the open sea and $-1.522 \pm 0.108 \text{ mol C m}^{-2} \text{ yr}^{-1}$ for the continental shelf margins (Chau et al., 2022). Air-sea CO₂ flux range from -4 to -86 mol m⁻² d⁻¹ (Bates and Mathis, 2009; Bates et al.,
245 2011; Rysgaard et al., 2012).

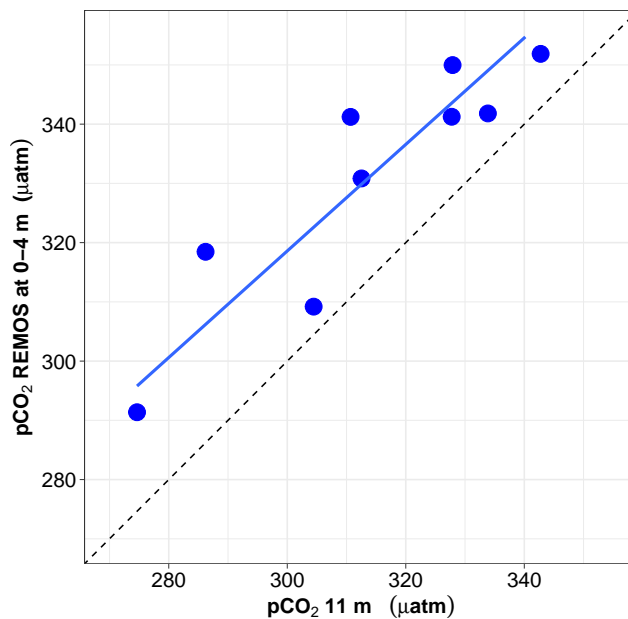


Figure 10. Relationship between surface pCO₂ [0-4 m] (estimated from pH and salinity-derived A_T) and pCO₂ at 11 m. Both values are expressed at *in situ* temperature. The mean and median difference between the two pCO₂ are about 17 µatm. The major axis regression line is shown in blue whereas the 1:1 relationship is depicted by a black dotted line.

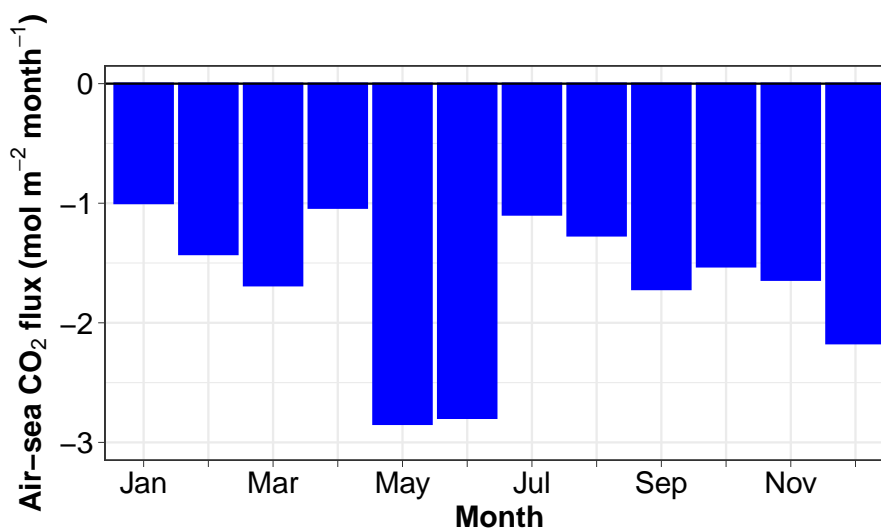


Figure 11. Air-sea CO₂ flux estimated using pCO₂ values collected at 11 m depth.



For example, the surface waters of the entire Godthåbsfjord (west Greenland) and adjacent continental shelf are undersaturated in CO_2 throughout the year (Meire et al., 2015). The average annual CO_2 uptake within the fjord is estimated to be $5.42 \text{ mol m}^{-2} \text{ yr}^{-1}$, indicating that the fjord system is a strong sink for CO_2 .

3.10 Saturation state of CaCO_3

250 The saturation state of CaCO_3 is subject to large interannual changes (Fig. 12). Ω_a never becomes lower than 1. Its it ranges between 1.4 in winter to 3 in summer.

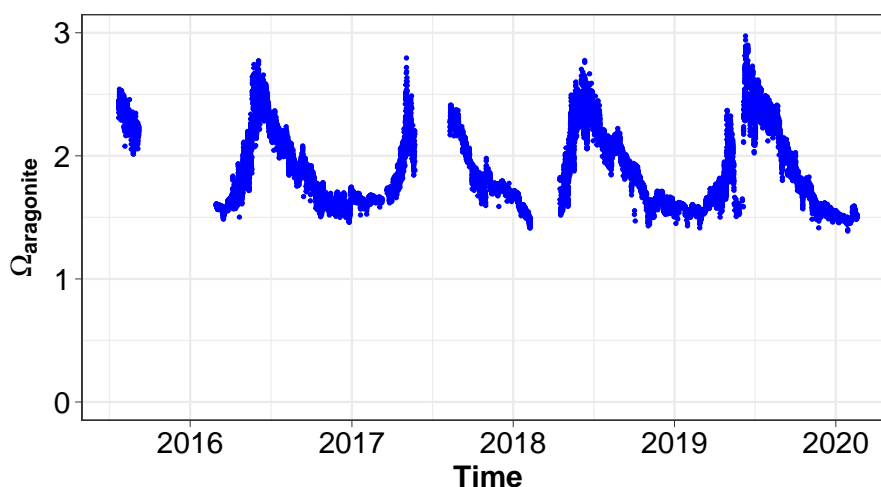


Figure 12. Time series of the aragonite saturation state calculated using pCO_2 and salinity-derived total alkalinity as input parameters.

4 Conclusion

Although measurements of the carbonate system have increased significantly in the Arctic Ocean, there is still a lack of high-frequency time series, also in the coastal zone. Autonomous time-series measurements in the Arctic involve a number of
255 challenges related to remoteness and harsh environment (Fischer et al., 2020). The most serious incidents our study faced related to system damages from iceberg collisions as well as frozen tubes delivering sea water to the land based measuring system. The remoteness and harsh environmental conditions made maintenance difficult especially during the polar winter and led to a discontinuous dataset. Even though we planned this dataset to become a real long-term dataset, unfortunate non-technical circumstances brought this time series to an end, preventing the assessment of interannual variability. Nevertheless,
260 it is unique by its high (hourly) frequency, coverage of all seasons, and duration (over 4 years).



The final data product provides information on a series of key questions on the dynamics and carbon cycling in a high-Arctic fjord. Several have been discussed above. Our results show that (1) the choice of formulations for calculating the dissociation constants of the carbonic acid remains unsettled, (2) the 12-m high water column is consistently stratified most of the time, (3) the calcium carbonate saturation state is subject to large seasonal changes but never reaches undersaturation, (4) this coastal site is a large CO₂ sink.

4.1 Data availability

Data are available on Zenodo during the review process (Gattuso et al., 2023): <https://doi.org/10.5281/zenodo.7714954>. The final version will be published on Pangaea after acceptance of the paper. The csv file "AWIPEV-CO2_v1.csv" comprises the following variables:

- 270 – Continuous variables (hourly means):
 - Date/time [UTC+0]: date and time at UTC+0
 - pressure_profiler [dbar]: hydrostatic pressure (profiler)
 - salinity_PSS78_profiler [unit]: salinity in situ (profiler)
 - salinity_PSS78_ferrybox [unit]: salinity (FerryBox)
 - 275 - temperature_ITS90_11m [°C]: temperature *in situ* (static at 11 m)
 - temperature_ITS90_profiler [°C]: temperature *in situ* (profiler)
 - temperature_ITS90_ferrybox [°C]: temperature (FerryBox)
 - temperature_ITS90_seafet_profiler [°C]: temperature SeaFET (profiler)
 - pco2_insitu_temperature_ferrybox [uatm]: partial pressure of CO₂ (FerryBox)
 - 280 - ph_insitu_temperature_profiler [total scale]: pH *in situ* at *in situ* temperature (profiler)
- Discrete variables:
 - ta_discrete [umolkg⁻¹]: total alkalinity *in situ* (discrete)
 - dic_discrete [umol kg⁻¹]: dissolved inorganic carbon *in situ* (discrete)
 - ph_discrete [total scale]: spectrophotometric pH *in situ* at *in situ* temperature (discrete)

285 *Author contributions.* JPG conceived the project. PF led the sensor implementation and underwater sensor maintenance. SA and PF maintained the FerryBox system, the instrumentation and the continuous data transfer. SA and JPG led data processing and analysis. JPG led the analysis and writing with contributions from SA and PF. JPG wrote the draft and coauthors contributed text and edits.



Competing interests. The authors declare that they have no conflict of interest.

Acknowledgements. Thanks are due to Robert Schlegel (Sorbonne Université) for his help with data upload, to Li-Qing Jiang (NOAA) for his advice about variable names and Mohammed Khamla for assistance with graphics. We are extremely grateful to the AWIPEV staff who made the continuous operation of the underwater observatory in such a remote location possible almost flawlessly until 2020. Such gratitude cannot be extended to the staff on duty in 2020. We thank the numerous divers from the AWI Centre for Scientific Diving for their invaluable assistance during the maintenance trips. We are indebted to Willem H. van de Poll who kindly provided nutrient data. We thank Ove Hermansen, Cathrine Lund Myhre, and Stephen Platt at Norwegian Institute for Air Research (NILU) for their assistance with atmospheric CO₂ data from the Zeppelin observatory, as well as the Integrated Carbon Observing System (ICOS)-Norway, Norwegian Research Council project NFR-207587, and the Norwegian Environment Agency. Atmospheric CO₂ data from Zeppelin is available from EBAS: <http://ebas.nilu.no>. This work has been supported by the Coastal Observing System for Northern and Arctic Seas (COSYNA), the two Helmholtz large-scale infrastructure projects ACROSS and MOSES, the French Polar Institute (IPEV) as well as the European Union's Horizon 2020 research and innovation projects Jericho-Next (No 871153 and 951799), INTAROS (No 727890) and FACE-IT (No 869154).

300 **Appendix A: Related datasets**

Longer (2012-2021) datasets are available for salinity and temperature (Fischer and colleagues). They are stored in the open access repository PANGAEA:

- 2012: <https://doi.org/10.1594/PANGAEA.896828>
- 2013: <https://doi.org/10.1594/PANGAEA.896822>
- 305 – 2014: <https://doi.org/10.1594/PANGAEA.896821>
- 2015: <https://doi.org/10.1594/PANGAEA.896771>
- 2016: <https://doi.org/10.1594/PANGAEA.896770>
- 2017: <https://doi.org/10.1594/PANGAEA.896170>
- 2018: <https://doi.org/10.1594/PANGAEA.897349>
- 310 – 2019: <https://doi.org/10.1594/PANGAEA.927607>
- 2020: <https://doi.org/10.1594/PANGAEA.929583>
- 2021: <https://doi.org/10.1594/PANGAEA.950174>



References

- Anderson, L., Ek, J., Ericson, Y., Humborg, C., Semiletov, I., Sundbom, M., and Ulfso, A.: Export of calcium carbonate corrosive waters
315 from the East Siberian Sea, *Biogeosciences*, 14, 1811–1823, 2017.
- Bakker, D. C. E., Pfeil, B., Landa, C. S., Metzl, N., Oapobrien, K. M., Olsen, A., Smith, K., Cosca, C., Harasawa, S., Jones, S. D.,
Nakaoka, S.-i., Nojiri, Y., Schuster, U., Steinhoff, T., Sweeney, C., Takahashi, T., Tilbrook, B., Wada, C., Wanninkhof, R., Alin, S. R.,
Balestrini, C. F., Barbero, L., Bates, N. R., Bianchi, A. A., Bonou, F., Boutin, J., Bozec, Y., Burger, E. F., Cai, W.-J., Castle, R. D., Chen,
L., Chierici, M., Currie, K., Evans, W., Featherstone, C., Feely, R. A., Fransson, A., Goyet, C., Greenwood, N., Gregor, L., Hankin, S.,
320 Hardman-Mountford, N. J., Harlay, J., Hauck, J., Hoppema, M., Humphreys, M. P., Hunt, C. W., Huss, B., Ibáñez, J. S. P., Johannessen,
T., Keeling, R., Kitidis, V., Körtzinger, A., Kozyr, A., Krasakopoulou, E., Kuwata, A., Landschützer, P., Lauvset, S. K., Lefèvre, N.,
Lo Monaco, C., Manke, A., Mathis, J. T., Merlivat, L., Millero, F. J., Monteiro, P. M. S., Munro, D. R., Murata, A., Newberger, T., Omar,
A. M., Ono, T., Paterson, K., Pearce, D., Pierrot, D., Robbins, L. L., Saito, S., Salisbury, J., Schlitzer, R., Schneider, B., Schweitzer, R.,
Sieger, R., Skjelvan, I., Sullivan, K. F., Sutherland, S. C., Sutton, A. J., Tadokoro, K., Telszewski, M., Tuma, M., van Heuven, S. M. A. C.,
325 Vandemark, D., Ward, B., Watson, A. J., and Xu, S.: A multi-decade record of high-quality fCO₂ data in version 3 of the Surface Ocean
CO₂ Atlas (SOCAT), *Earth Syst. Sci. Data*, 8, 383–413, 2016.
- Bates, N., Cai, W.-J., and Mathis, J.: The ocean carbon cycle in the western Arctic ocean: distributions and air-sea fluxes of carbon dioxide,
Oceanography, 24, 186–201, 2011.
- Bates, N. R. and Mathis, J. T.: The Arctic Ocean marine carbon cycle: evaluation of air-sea CO₂ exchanges, ocean acidification impacts and
330 potential feedbacks, *Biogeosciences*, 6, 2433–2459, 2009.
- Bresnahan, P. J., Martz, T., Takeshita, Y., Johnson, K., and LaShomb, M.: Best practices for autonomous measurement of seawater pH with
the Honeywell Durafet, *Methods in Oceanography*, 9, 44–60, 2014.
- Chau, T., Gehlen, M., and Chevallier, F.: A seamless ensemble-based reconstruction of surface ocean pCO₂ and air–sea CO₂ fluxes over the
global coastal and open oceans, *Biogeosciences*, 19, 1087–1109, 2022.
- 335 Chen, B., Cai, W.-J., and Chen, L.: The marine carbonate system of the Arctic Ocean: Assessment of internal consistency and sampling
considerations, summer 2010, *Mar. Chem.*, 176, 174–188, 2015.
- Chierici, M. and Fransson, A.: Calcium carbonate saturation in the surface water of the Arctic Ocean: undersaturation in freshwater influenced
shelves, *Biogeosciences*, 6, 2421–2431, 2009.
- Comeau, S., Gattuso, J.-P., Nisumaa, A.-M., and Orr, J.: Impact of aragonite saturation state changes on migratory pteropods, *Proc. R. Soc.*
340 *Lond. B*, 279, 732–738, 2011.
- De Carlo, E., Mousseau, L., Passafiume, O., Drupp, P., and Gattuso, J.-P.: Carbonate chemistry and air–sea CO₂ flux in a NW Mediterranean
Bay over a four-year period: 2007–2011, *Aquatic Geochemistry*, 19, 399–442, 2013.
- Dickson, A. G. and Riley, J. P.: The effect of analytical error on the evaluation of the components of the aquatic carbon-dioxide system, *Mar.*
Chem., 6, 77–85, 1978.
- 345 Dickson, A. G., Sabine, C. L., and Christian, J. R.: Guide to best practices for ocean CO₂ measurements, PICES Special Publication, 3,
1–191, 2007.
- DOE: Handbook of methods for the analysis of the various parameters of the carbon dioxide system in sea water, Carbon Dioxide Information
Analysis Center, Oak Ridge National Laboratory, 1994.



- Dong, Y., Yang, M., Bakker, D. C. E., Liss, P. S., Kitidis, V., Brown, I., Chierici, M., Fransson, A., and Bell, T. G.: Near-surface stratification
350 due to ice melt biases arctic air-sea CO₂ flux estimates, *Geophys. Res. Lett.*, 48, 2021.
- Edmond, J. M.: High precision determination of titration alkalinity and total carbon dioxide content of sea water by potentiometric titration,
Deep-Sea Res., 17, 737–750, 1970.
- Fischer, P., Schwanitz, M., Loth, R., Posner, U., Brand, M., and Schröder, F.: First year of practical experiences of the new Arctic AWIPEV-
COSYNA cabled Underwater Observatory in Kongsfjorden, Spitsbergen, *Ocean Science*, 13, 259–272, 2017.
- 355 Fischer, P., Brix, H., Baschek, B., Kraberg, A., Brand, M., Cisewski, B., Riethmüller, R., Breitbach, G., Möller, K., Gattuso, J.-P., Posner, U.,
Alliouane, S., Loth, R., Van De Poll, W., and Witbaard, R.: Operating cabled underwater observatories in rough shelf-sea environments: a
technological challenge, *Front. Mar. Sci.*, 7, 551, 2020.
- Fox-Kemper, B., Hewitt, H., Xiao, C., Aðalgeirsdóttir, G., Drijfhout, S., Edwards, T., Golledge, N., Hemer, M., Kopp, R., Krinner, G., Mix,
A., Notz, D., Nowicki, S., Nurhati, I., Ruiz, L., Sallée, J.-B., Slangen, A., and Yu, Y.: Ocean, cryosphere and sea level change, in: *Climate*
360 *Change 2021: The Physical Science Basis. Contribution of Working Group I to the Sixth Assessment Report of the Intergovernmental*
Panel on Climate Change, edited by Masson-Delmotte, V., Zhai, P., Pirani, A., Connors, S., Péan, C., Berger, S., Caud, N., Chen, Y.,
Goldfarb, L., Gomis, M., Huang, M., Leitzell, K., Lonnoy, E., Matthews, J., Maycock, T., Waterfield, T., Yelekçi, O., Yu, R., and Zhou,
B., 2021.
- Fransson, A., Chierici, M., Nomura, D., Granskog, M., Kristiansen, S., Martma, T., and Nehrke, G.: Effect of glacial drainage water on
365 the CO₂ system and ocean acidification state in an Arctic tidewater-glacier fjord during two contrasting years, *J. Geophys. Res.*, 120,
2413–2429, 2015.
- Gattuso, J.-P., Epitalon, J.-M., Lavigne, H., and Orr, J.: seacarb: seawater carbonate chemistry. R package version 3.2.16, <https://CRAN.R-project.org/package=seacarb>, 2021.
- Gattuso, J.-P., Alliouane, S., and Fischer, P.: High-frequency, year-round time series of the carbonate chemistry in a high-Arctic fjord (Sval-
370 bard) (0.9), *Zenodo*, <https://doi.org/10.5281/zenodo.7714954>, 2023.
- Gerland, S. and Renner, A. H.: Sea-ice mass-balance monitoring in an Arctic fjord, *Annals of Glaciology*, 46, 435–442, 2007.
- Ho, D. T., Law, C. S., Smith, M. J., Schlosser, P., Harvey, M., and Hill, P.: Measurements of air-sea gas exchange at high wind speeds in the
Southern Ocean: Implications for global parameterizations, *Geophys. Res. Lett.*, 33, 2006.
- Hunt, C., Salisbury, J., Vandemark, D., Abmann, S., Fietzek, P., Melrose, C., Wanninkhof, R., and Azetsu-Scott, K.: Variability of USA East
375 Coast surface total alkalinity distributions revealed by automated instrument measurements, *Mar. Chem.*, 232, 103 960, 2021.
- IOC, SCOR, and IAPSO: The international thermodynamic equation of seawater–2010: calculation and use of thermodynamic properties,
Intergovernmental Oceanographic Commission, Manuals and Guides, 56, 196, 2010.
- Jakobsson, M., Grantz, A., Kristoffersen, Y., and Macnab, R.: Bathymetry and physiography of the Arctic Ocean and its constituent seas, in:
The organic carbon cycle in the Arctic Ocean, edited by Stein, R. and Macdonald, R. W., pp. 1–6, Springer, Berlin, 2004.
- 380 Jiang, L.-Q., Pierrot, D., Wanninkhof, R., Feely, R. A., Tilbrook, B., Alin, S., Barbero, L., Byrne, R. H., Carter, B. R., Dickson, A. G.,
Gattuso, J.-P., Greeley, D., Hoppema, M., Humphreys, M. P., Karstensen, J., Lange, N., Lauvset, S. K., Lewis, E. R., Olsen, A., Pérez,
F. F., Sabine, C., Sharp, J. D., Tanhua, T., Trull, T. W., Velo, A., Allegra, A. J., Barker, P., Burger, E., Cai, W.-J., Chen, C.-T. A., Cross, J.,
Garcia, H., Hernandez-Ayon, J. M., Hu, X., Kozyr, A., Langdon, C., Lee, K., Salisbury, J., Wang, Z. A., and Xue, L.: Best practice data
standards for discrete chemical oceanographic observations, *Front. Mar. Sci.*, 8, 705 638, 2022.
- 385 Kelley, D. and Richards, C.: oce: analysis of oceanographic data. R package version 1.3-0, <https://CRAN.R-project.org/package=oce>, 2021.



- 390 Kwiatkowski, L., Torres, O., Bopp, L., Aumont, O., Chamberlain, M., Christian, J., Dunne, J., Gehlen, M., Ilyina, T., John, J., Lenton, A.,
Li, H., Lovenduski, N., Orr, J., Palmieri, J., Santana-Falcón, Y., Schwinger, J., Séférian, R., Stock, C., Tagliabue, A., Takano, Y., Tjiputra,
J., Toyama, K., Tsujino, H., Watanabe, M., Yamamoto, A., Yool, A., and Ziehn, T.: Twenty-first century ocean warming, acidification,
deoxygenation, and upper-ocean nutrient and primary production decline from CMIP6 model projections, *Biogeosciences*, 17, 3439–3470,
2020.
- Lantuit, H., Overduin, P. P., Couture, N., Wetterich, S., Aré, F., Atkinson, D., Brown, J., Cherkashov, G., Drozdov, D., Forbes, D. L., Graves-
Gaylord, A., Grigoriev, M., Hubberten, H.-W., Jordan, J., Jorgenson, T., Ødegård, R. S., Ogorodov, S., Pollard, W. H., Rachold, V.,
Sedenko, S., Solomon, S., Steenhuisen, F., Streletskaia, I., and Vasiliev, A.: The Arctic Coastal Dynamics Database: a new classification
scheme and statistics on Arctic permafrost coastlines, *Estuar. Coasts*, 35, 383–400, 2012.
- 395 Lauvset, S. K., Lange, N., Tanhua, T., Bittig, H. C., Olsen, A., Kozyr, A., Alin, S., Álvarez, M., Azetsu-Scott, K., Barbero, L., Becker, S.,
Brown, P. J., Carter, B. R., da Cunha, L. C., Feely, R. A., Hoppema, M., Humphreys, M. P., Ishii, M., Jeansson, E., Jiang, L.-Q., Jones,
S. D., Lo Monaco, C., Murata, A., Müller, J. D., Pérez, F. F., Pfeil, B., Schirnack, C., Steinfeldt, R., Suzuki, T., Tilbrook, B., Ulfso, A.,
Velo, A., Woosley, R. J., and Key, R. M.: GLODAPv2.2022: the latest version of the global interior ocean biogeochemical data product,
Earth Syst. Sci. Data, 14, 5543–5572, 2022.
- 400 Lee, K., Kim, T.-W., Byrne, R. H., Millero, F. J., Feely, R. A., and Liu, Y.-M.: The universal ratio of boron to chlorinity for the North Pacific
and North Atlantic oceans, *Geochim. Cosmochim. Acta*, 74, 1801–1811, 2010.
- Lueker, T. J., Dickson, A., and Keeling, C. D.: Ocean pCO₂ calculated from dissolved inorganic carbon, alkalinity, and equations for K₁ and
K₂: validation based on laboratory measurements of CO₂ in gas and seawater at equilibrium, *Mar. Chem.*, 70, 105–119, 2000.
- Maturilli, M.: Continuous meteorological observations at station Ny-Ålesund (2011-08 et seq), PANGAEA, p. 23–46, 2020.
- 405 McLaughlin, K., Dickson, A., Weisberg, S., Coale, K., Elrod, V., Hunter, C., Johnson, K., Kram, S., Kudela, R., Martz, T., Negrey, K.,
Passow, U., Shaughnessy, F., Smith, J., Tadesse, D., Washburn, L., and Weis, K.: An evaluation of ISFET sensors for coastal pH monitoring
applications, *Regional Studies in Marine Science*, 12, 11–18, 2017.
- Mehrbach, C., Culbertson, C. H., Hawley, J. E., and Pytkowicz, R. M.: Measurement of the apparent dissociation constants of carbonic acid
in seawater at atmospheric pressure, *Limnol. Oceanogr.*, 18, 897–907, 1973.
- 410 Meire, L., Sjøgaard, D., Mortensen, J., Meysman, F., Soetaert, K., Arendt, K., Juul-Pedersen, T., Blicher, M., and Rysgaard, S.: Glacial
meltwater and primary production are drivers of strong CO₂ uptake in fjord and coastal waters adjacent to the Greenland Ice Sheet,
Biogeosciences, 12, 2347–2363, 2015.
- Menard, H. W. and Smith, S. M.: Hypsometry of ocean basin provinces, *J. Geophys. Res.*, 71, 4305–4325, 1966.
- Miller, L. A., Burgers, T. M., Burt, W. J., Granskog, M. A., and Papakyriakou, T. N.: Air-sea CO₂ flux estimates in stratified arctic coastal
415 waters: how wrong can we be, *Geophys. Res. Lett.*, 46, 235–243, 2019.
- Millero, F. J., Pierrot, D., Lee, K., Wanninkhof, R., Feely, R., Sabine, C. L., Key, R. M., and Takahashi, T.: Dissociation constants for carbonic
acid determined from field measurements, *Deep Sea Research Part I: Oceanographic Research Papers*, 49, 1705–1723, 2002.
- Nondal, G., Bellerby, R. G. J., Olsen, A., Johannessen, T., and Olafsson, J.: Optimal evaluation of the surface ocean CO₂ system in the
northern North Atlantic using data from voluntary observing ships, *Limnol. Oceanogr. Methods*, 7, 109–118, 2009.
- 420 Organization, I. H.: Limits of oceans and seas, Special Publication, 23, 1–45, 1953.
- Orr, J., Epitalon, J.-M., Dickson, A., and Gattuso, J.-P.: Routine uncertainty propagation for the marine carbon dioxide system, *Mar. Chem.*,
207, 84–107, 2018.



- O'Neill, B., Oppenheimer, M., Warren, R., Hallegatte, S., Kopp, R., Pörtner, H., Scholes, R., Birkmann, J., Foden, W., Licker, R., Mach, K., Marbaix, P., Mastrandrea, M., Price, J., Takahashi, K., van Ypersele, J.-P., and Yohe, G.: IPCC reasons for concern regarding climate change risks, *Nat. Clim. Change*, 7, 28–37, 2017.
- Papadimitriou, S., Loucaides, S., Rérolle, V. M., Kennedy, P., Achterberg, E. P., Dickson, A. G., Mowlem, M., and Kennedy, H.: The stoichiometric dissociation constants of carbonic acid in seawater brines from 298 to 267 K, *Geochim. Cosmochim. Acta*, 220, 55–70, 2018.
- Pavlova, O., Gerland, S., and Hop, H.: Changes in sea-ice extent and thickness in Kongsfjorden, Svalbard (2003–2016), in: *The ecosystem of Kongsfjorden, Svalbard*, edited by Hop, H. and Wiencke, C., pp. 105–136, Springer, Cham, 2019.
- Perez, F. F. and Fraga, F.: Association constant of fluoride and hydrogen ions in seawater, *Mar. Chem.*, 21, 161–168, 1987.
- Rysgaard, S., Mortensen, J., Juul-Pedersen, T., Sørensen, L., Lennert, K., Sjøgaard, D., Arendt, K., Blicher, M., Sejr, M., and Bendtsen, J.: High air-sea CO₂ uptake rates in nearshore and shelf areas of Southern Greenland: Temporal and spatial variability, *Mar. Chem.*, 128–129, 26–33, 2012.
- Shiklomanov, I.: Comprehensive assessment of the freshwater resources of the world: assessment of water resources and water availability in the world, World Meteorological Organization, Geneva, 1998.
- Stein, R. and Macdonald, R. W.: Organic carbon budget: Arctic Ocean vs. global ocean, in: *The organic carbon cycle in the Arctic Ocean*, edited by Stein, R. and Macdonald, R. W., pp. 315–322, Springer, Berlin, 2004.
- Sulpis, O., Lauvset, S., and Hagens, M.: Current estimates of K₁* and K₂* appear inconsistent with measured CO₂ system parameters in cold oceanic regions, *Ocean Science*, 16, 847–862, 2020.
- Takahashi, T., Sutherland, S. C., Sweeney, C., Poisson, A., Metzl, N., Tilbrook, B., Bates, N., Wanninkhof, R., Feely, R. A., and Sabine, C.: Global sea-air CO₂ flux based on climatological surface ocean pCO₂, and seasonal biological and temperature effects, *Deep-Sea Res. II*, 49, 1601–1622, 2002.
- Vihtakari, M.: ggOceanMaps: plot data on oceanographic maps using 'ggplot2'. R package version 1.3.4, <https://CRAN.R-project.org/package=ggOceanMaps>, 2022.
- Wassmann, P., Duarte, C., Agustí, S., and Sejr, M.: Footprints of climate change in the Arctic marine ecosystem, *Glob. Change Biol.*, 17, 1235–1249, 2010.
- Zhang, Y., Yamamoto-Kawai, M., and Williams, W.: Two decades of ocean acidification in the surface waters of the Beaufort Gyre, Arctic Ocean: effects of sea ice melt and retreat from 1997–2016, *Geophys. Res. Lett.*, 47, e60119, 2020.